Subharmonic Entrainment of Kerr Breather Solitons

Daniel C. Cole* and Scott B. Papp
Time & Frequency Division, NIST Boulder, Boulder, Colorado 80305, USA

(Received 25 July 2019; published 25 October 2019)

We predict subharmonic entrainment of breather-soliton oscillations to a periodic perturbation at the round-trip time T_R in Kerr-nonlinear optical resonators; an integer ratio $T_b/T_R = N \gg 1$ results for breathing period T_b. Rigid entrainment is observed with intermediate finesse ($\mathcal{F} \sim 30$–40) for N up to 20, and we propose a way to realize higher entrainment ratios at higher finesse. This nontrivial synchronization across the widely separated timescales of the photon lifetime and round-trip time points to a new direction for research in this field and may find application, for example, in the measurement of a pulse train repetition rate that is electronically inaccessible.

DOI: 10.1103/PhysRevLett.123.173904

Optical solitons generated in high-Q Kerr-nonlinear microresonators [*microcombs*, see Fig. 1(a)] [1,2] are a promising candidate for photonic integration of optical frequency comb technology, which will enable a wide variety of applications through the portable synthesis, control, and measurement of optical frequencies. The rich nonlinear dynamics of microcombs are fundamentally interesting and provide opportunities to tailor microcomb properties for applications. Some facets that have been investigated in depth are the effects of dispersion [3,4], mode structure [5–8], and Raman scattering [9–12]; thermal effects [13–15]; and spontaneous ordering of copropagating solitons [16,17].

Under certain conditions the amplitude and duration of microcomb solitons oscillate, or breathe, in time. This manifests as a modulation of the pulse energies in the out-coupled pulse train, depicted in Fig. 1(b); typically the oscillation period T_b is much larger than the resonator round-trip time T_R. *Breather solitons* have been investigated experimentally [18–21] and are well known outside of the microcomb field (e.g. [22,23]), but the emphasis for microcomb applications has mostly remained on non-breathing solitons. Here, we focus on breather solitons and propose a new type of spontaneous synchronization in microcombs: subharmonic entrainment of breather oscillations to the round-trip time.

The fundamental timescale for evolution of the field in a high-finesse cavity is the photon lifetime $\tau_{\mathrm{ph}} \gg T_R$, and it has generally been found that round-trip-time effects do not need to be included to successfully model most microcomb properties. However, small perturbations to nonlinear systems can lead to qualitatively new behavior, and in microcombs such a perturbation is provided by periodic out-coupling and interference with the pump field. We explore one possible effect of this perturbation by numerically investigating subharmonic entrainment of breather oscillations to the round-trip time such that an integer ratio

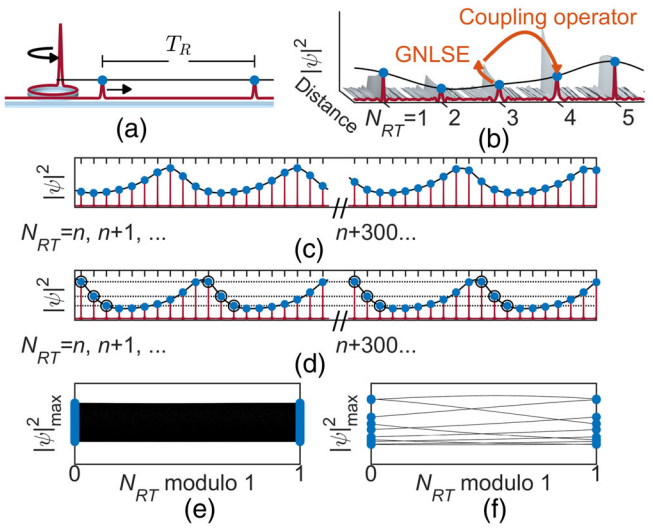

FIG. 1. The system under study. (a) Solitons in a Kerr-nonlinear ring resonator, with bus waveguide. The intensity profile $|\psi|^2$ of a circulating soliton is shown in red, with two out-coupled pulses separated by the round-trip time T_R; amplitudes indicated by blue dots. (b) An Ikeda-map simulation of a breather soliton conducted with parameters $\alpha = 4.5$, $F^2 = 10$, $\beta_2 = -0.2$, and $\mathcal{F} = 12$. The out-coupled pulse train is shown in red as a function of round-trip times N_{RT}, and the gray surface plot depicts evolution (into the page) within each round trip according to the GNLSE. Blue dots mark amplitudes of out-coupled pulses $|\psi|^2_{\max}$, and the black curve is a conceptual guide. (c),(d) Depictions of free [(c), $F^2 = 9$] and entrained [(d), $F^2 = 10$, $N = 10$] breather oscillations for $\alpha = 4.5$, $\beta_2 = -0.02$, and $\mathcal{F} = 24.69$. In (d) we show the periodicity of the breather amplitudes for three different points. (e),(f) Breather amplitudes as a function of drive phase (N_{RT} modulo 1) over a simulation of ~8000 round trips in the free (e) and entrained (f) cases. In (f) the oscillator assumes $N = 10$ discrete positions for each value of the drive phase; no such order exists in (e).

$N = T_b/T_R \gg 1$ arises. This entrainment would represent a nontrivial synchronization between slow ($\sim$ photon lifetime) and fast ($\sim$ round-trip time) dynamics for microcombs, which to our knowledge has not previously been proposed, and would demonstrate spontaneous violation of the discrete time-translation symmetry (for $t \to t + nT_R$, $n = 1, 2, \ldots$) of the equations of motion for the intracavity field. Our work builds upon previous investigations of subharmonic entrainment in a variety of systems [24–27] and on previous studies of period doubling in passive [28] and lasing [29] fiber-loop cavities, and takes place alongside recent discoveries of spontaneous violation of discrete time-translation symmetry in quantum systems [30–32].

Our numerical investigations, depicted schematically in Fig. 1(b), reveal subharmonic entrainment of breather oscillations to the round-trip time; the effect is illustrated in Figs. 1(c)–1(f). We explore a regime of intermediate finesse because this strengthens the round-trip-time perturbation and makes simulations practical. We present results for $T_b/T_R = N$ up to 13, and find that entrainment persists over a range of system parameters, and even as they are dynamically varied. Our simulations indicate that the strength of entrainment decays exponentially with increasing finesse, so we discuss possible routes towards realization of the effect at higher finesse. As an example, we show that the introduction of fourth-order dispersion immediately allows us to extend the effect to $N = 20$. This ratio is high enough to use the effect to electronically measure, for example, a microcomb repetition rate of 1 THz by measuring subharmonically-entrained breather oscillations at 50 GHz. This could greatly simplify the integration of microcombs for applications. We conclude by discussing prospects for experimental realization of entrained breather oscillations.

The canonical model for microcomb dynamics is the Lugiato-Lefever equation (LLE) [33–38], which has been successful in reproducing microcomb experimental results and informing system design. One version of the equation reads [38]

$$\frac{\partial \psi}{\partial \tau} = -(1 + i\alpha)\psi + i|\psi|^2\psi - i\frac{\beta_2}{2}\frac{\partial^2 \psi}{\partial \theta^2} + F. \quad (1)$$

Here, $\psi(\theta, \tau)$ and F represent the intracavity field envelope and pump strength, and α and β_2 represent the detuning of the laser from the cavity ($\alpha > 0$ for a laser of lower frequency than the nearby cavity mode) and the second-order dispersion ($\beta_2 < 0$ for anomalous dispersion). The field ψ is defined over a comoving azimuthal angle $-\pi < \theta < \pi$ and evolves over a slow time $\tau = t/2\tau_{\mathrm{ph}}$. Normalization is provided in the Supplemental Material (SM) [39].

The LLE is an approximate model for microcomb dynamics that emerges in the high-finesse limit. Because it exhibits continuous time-translation symmetry in the slow time τ, the LLE cannot reveal effects arising from the periodic round-trip time perturbation. We explore these effects with an *Ikeda map*, a more fundamental model from which the LLE may be obtained [41–44] (see Ref. [44] for the form of the equations used here). In this model, the field $\psi_n(\theta, s)$ evolves over the nth round trip as a function of a normalized spatial coordinate s according to a generalized nonlinear Schrodinger equation (GNLSE, ubiquitous in describing propagation in Kerr-nonlinear, dispersive media [45]) of the form

$$\frac{\partial \psi}{\partial s} = -(1 - \eta)\psi + i|\psi|^2\psi - i\frac{\beta_2}{2}\frac{\partial^2 \psi}{\partial \theta^2}, \quad (2)$$

where the round trip corresponds to a distance $\Delta s = \pi/\mathcal{F}$. The field at the beginning of the next round trip is then obtained by incorporating out-coupling and pumping via

$$\psi_{n+1}(\theta, 0) = e^{-i(\pi/\mathcal{F})\alpha}\left(1 - \frac{\pi\eta}{\mathcal{F}}\right)\psi_n(\theta, \pi/\mathcal{F}) + \frac{\pi}{\mathcal{F}}F. \quad (3)$$

This model is depicted conceptually in Fig. 1(b). To define the Ikeda map relative to the LLE, we specify the resonator finesse $\mathcal{F} = 2\pi\tau_{\mathrm{ph}}/T_R$ and the coupling ratio $\eta = \tau_{\mathrm{ph}}\Delta\omega_{\mathrm{ext}}$, which quantifies the relative magnitudes of external coupling with rate $\Delta\omega_{\mathrm{ext}}$ and internal dissipation with rate $\Delta\omega_{\mathrm{int}} = 1/\tau_{\mathrm{ph}} - \Delta\omega_{\mathrm{ext}}$. This Ikeda map reduces to Eq. (1) in the high-finesse limit [44].

In this Letter we explore the limiting case $\eta = 1$, well approximated by a resonator that is strongly overcoupled. This is natural because we consider a regime in which the finesse is much lower than the value allowed by, e.g. critical coupling ($\eta = 1/2$) of a typical microresonator, and setting $\eta = 1$ maximizes the strength of the periodic round-trip-time perturbation. However, we also verify that subharmonic entrainment persists for smaller, experimentally realistic coupling ratios, e.g. $\eta = 0.95$.

Below, we report on the results of our use of Ikeda map simulations to study breather solitons. A detailed description of these simulations is provided in the SM [39].

We consider a breather soliton at detuning $\alpha = 4.5$, pump power $F^2 = 10$, dispersion $\beta_2 = -0.02$, and coupling ratio $\eta = 1$. We first examine the effect of departing from the high-finesse limit. In Fig. 2(a) we show the breathing period as a function of the resonator finesse; the period changes little relative to the photon lifetime as the finesse is varied. We find that breather period $\mathcal{T}_b$ expressed in units of τ_{ph} is well described by $\mathcal{T}_b(\mathcal{F}) = \mathcal{T}_{b,\mathrm{LLE}} - A/\mathcal{F}$, where $A \sim 3.47$ and $\mathcal{T}_{b,\mathrm{LLE}}$ is the breather period in the high-finesse limit. From preliminary investigations of other points (described by detuning α, pump power F^2, dispersion β_2, and coupling ratio η), it appears that this behavior is not universal, and other powers of $\mathcal{F}$ may be required for agreement with the observations.

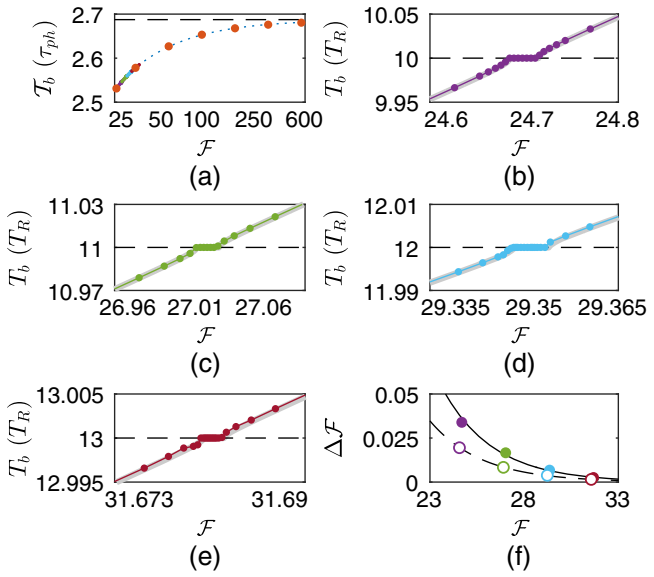

FIG. 2. Exploration of breather entrainment. (a) Breather period $\mathcal{T}_b$ (units of τ_{ph}) as a function of finesse, with the high-finesse limit shown in dashed black. The fit shown in dotted blue is obtained from the simulation results indicated by orange dots and is described in the text. The data points presented in parts (b)–(e) are also included. (b)–(e) Breather period T_b (units of T_R) as a function of finesse over several intervals where it approaches an integer. Fits using an injection locking model are shown in solid gray. (f) Locking range $\Delta\mathcal{F}$ as a function of finesse for $\eta = 1$ ($\eta = 0.95$) shown by filled (empty) dots, obtained from the injection-locking model, with a decaying exponential fit indicated by the solid (dashed) line.

The breather period T_b expressed in units of T_R varies greatly over the range $25 \leq \mathcal{F} \leq 600$ through the relation $T_b = \mathcal{T}_b\mathcal{F}/2\pi$ (we use the symbols $\mathcal{T}_b$ and T_b for the breather period expressed in units of τ_{ph} and T_R, respectively). In Figs. 2(b)–2(e) we present calculations of T_b for intervals of finesse over which it approaches an integer. The data exhibit plateaus of subharmonic entrainment, where T_b deviates from the expected value and rigidly snaps to an integer.

Figures 2(b)–2(e) include fits to an injection locking model [46] that predicts the difference between the breather frequency $f_b = 1/T_b$ and the subharmonic perturbation frequency f_{rep}/N in terms of a free-running breather frequency $f_{b,0}(\mathcal{F}) = 1/T_{b,0}(\mathcal{F})$ and a locking bandwidth δ:

$$f_b = f_{\mathrm{rep}}/N + \mathrm{sign}(\Delta) \times \mathrm{Re}\sqrt{\Delta^2 - \delta^2}, \qquad (4)$$

where $\Delta = f_{b,0}(\mathcal{F}) - f_{\mathrm{rep}}/N$ and δ is determined by fitting the data. For Figs. 2(b)–2(e) $f_{b,0}(\mathcal{F})$ is assumed locally linear and is obtained by fitting data far from the plateau. We plot the locking range $\Delta\mathcal{F}$ determined from the fit as a function of the finesse in Fig. 2(f), with a fit to a decaying exponential. This rapid decrease is expected for several reasons: First, the periodic perturbation becomes weaker with increasing finesse. Second, we expect the system's sensitivity to shifts in the timing of out-coupling and pumping relative to a hypothetical oscillation envelope (represented conceptually by the black curves in Fig. 1) to be related to $\partial|\psi|^2_{\mathrm{max}}/\partial N_{\mathrm{RT}}$, where $|\psi|^2_{\mathrm{max}}$ is the amplitude of the breather envelope and N_{RT} is the slow time in units of T_R. This sensitivity will decrease as T_b increases with increasing finesse.

To verify that subharmonic entrainment does not occur solely at the limit $\eta = 1$, we repeat the simulations described above for $\eta = 0.95$. The locking range calculated from these simulations is also presented in Fig. 2(f), and a full presentation and discussion of the results is given in the SM [39]. These results indicate that, as expected, the effect occurs at $\eta = 0.95$ but is slightly weaker than for $\eta = 1$, attributable to the reduced strength of the perturbation with smaller η.

We next investigate the plateaus of subharmonic entrainment with $N = 10$ for $\eta = 1$ as a function of the pump power F^2 and detuning α and present the results in Fig. 3. Figure 3(a) shows entrainment plateaus as a function of F^2 and α, with fits to Eq. (4). For F^2 we use spline interpolation between data far from the plateau to approximate $f_{b,0}$, which allows us to carry out the fit without knowing the dependence of $f_{b,0}$ on F^2. For α, we lack data

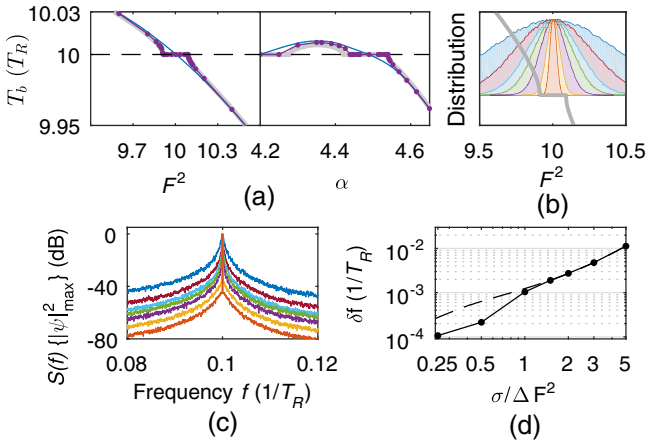

FIG. 3. Persistence of subharmonic entrainment with variation of F^2 and α. (a) Entrainment plateaus for variation of F^2 and α, with approximations of $T_{b,0}$ (blue) and fit to the injection-locking model (gray) obtained as described in the text. (b)–(d) Rigidity of entrainment when F^2 is dynamically varied using additive white Gaussian noise. (b) Histogram of F^2 values for seven simulations, with the fit from part a for scale. (c) Calculated spectra of breather amplitudes after observation over the second half of a simulation of 2^{19} round trips. Colors correspond to (b). The spectra are scaled to the same peak amplitude; spectra obtained for narrower F^2 distributions have larger coherent spikes at $f = 0.1/T_R$. (d) Thirty-dB width δf of the spectral peak at $f = 0.1/T_R$, calculated with resolution bandwidth $\sim 1 \times 10^{-4}/T_R$, as a function of the ratio of the standard deviation σ of the F^2 values to the locking range ΔF^2. The model indicated by the dashed line is described in the text.

on the free-running frequency $f_{b,0}(\alpha)$ below the plateau centered near $\alpha = 4.5$ (as all these data are strongly pulled), so we use the data above the plateau to generate an initial fit, and then use this fit to approximate the free-running frequencies $f_{b,0}(\alpha)$ over the full α interval. These fits provide qualitative approximations.

We also explore the effect of dynamical variations of F^2. We calculate the spectrum of the breather amplitudes $|\psi|^2_{\max}$ in the presence of normally-distributed time-varying F^2 values with standard deviations σ up to $5\Delta F^2$, where $\Delta F^2 = 0.087$ is the (half width) locking range obtained from Fig. 3(a); this value $5\Delta F^2$ is ~4% of the mean $F_0^2 = 10.0034$. Figures 3(b)–3(d) summarize the results. Figure 3(d) shows the thirty-dB linewidth of the breathing frequency as a function of σ, with a phenomenological model of the tone as a Lorentzian that is sampled with the appropriate resolution bandwidth and with linewidth proportional to $\sigma^{1.8}$. One arrives at a model in which the linewidth is proportional to σ^2 by assuming that the breathing frequency varies linearly with F^2, noting then that the power spectrum of breather-frequency fluctuations is proportional to σ^2, and observing that for white noise the linewidth is proportional to this spectrum [47]. That $\sigma^{1.8}$ provides a better fit to the data at high σ may be due to the fact that the breathing frequency does not actually vary linearly with F^2. The model agrees well with the data at high σ, but at low σ the data drop below the model, indicating a qualitative change as subharmonic entrainment stabilizes the breathing frequency.

In this initial study we have investigated a regime of intermediate finesse $\mathcal{F} \sim 30$, and conducting detailed Ikeda-map investigations for significantly higher values of the finesse is impractical. However, the finesse of microresonators is typically above 1000, and lowering the finesse increases the threshold power for comb generation. Moreover, we have seen that the strength of subharmonic entrainment falls exponentially with increasing finesse. Routes for overcoming this apparent obstacle could be investigated in future theoretical and experimental work. We have investigated a single LLE point in depth—this leaves the remainder of parameter space open for exploration. Moreover, there are effects that have been investigated within the context of the LLE that could be used to strengthen the effect, including Raman scattering, other higher-order nonlinearities, and higher-order dispersion. Additionally, azimuthally varying the nonlinear, dissipative, or dispersive properties of the resonator could increase the strength of round-trip-time effects (e.g. [48]). Finally, the coupling rate $\Delta\omega_{\text{ext}}$ could be spectrally varied so that the round-trip-time perturbation at the pump frequency is strong while out-coupling of the other comb modes is weaker, reducing increases in threshold power that come with lower finesse.

As an example, we consider that sharpening the breather oscillation to increase the sensitivity $\partial|\psi|^2_{\max}/\partial N_{\text{RT}}$ may help realize this effect at higher finesse. To test this idea we incorporate fourth-order dispersion into the LLE and the GNLSE [Eqs. (1) and (2)] by adding the term $+i(\beta_4/4!)(\partial^4\psi/\partial\theta^4)$ to the right-hand sides of these equations (see SM for normalization of β_4 [39]). Including β_4 with sign opposite to β_2 can reduce the mode-dependent detuning far from the pump (see [4]), facilitating broad bandwidth, temporal pulse compression, and high peak power, but only for a pulse that already has sufficient bandwidth to sample the reduced detuning—therefore temporal narrowing and increased peak power occurs for pulses that are already temporally short, i.e., when the breather is near its peak amplitude. An LLE simulation of the breather with $\beta_2 = -0.02$ and $\beta_4 = 8 \times 10^{-6}$ reveals sharper and higher-amplitude oscillations than in the case $\beta_4 = 0$. Ikeda map simulations of this breather reveal greater than tenfold improvement in the entrainment locking range, as depicted in Fig. 4. The improved locking range allows us to observe the effect up to at least a locking ratio of $N = 20$.

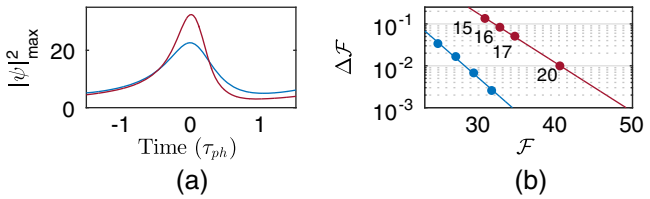

FIG. 4. Extension of subharmonic entrainment to higher finesse. (a) LLE simulations of a breather soliton for $\beta_4 = 8 \times 10^{-6}$ (red) and $\beta_4 = 0$ (blue). Fourth-order dispersion sharpens the breather oscillation. (b) Locking range $\Delta\mathcal{F}$ observed in Ikeda-map simulations of the two breathers from part (a). Including $\beta_4 = 8 \times 10^{-6}$ both shifts the locking-range curve up and reduces its slope; locking ratios N for $\beta_4 \neq 0$ are indicated next to the data points.

This increased locking ratio suggests one application for subharmonically-entrained breather solitons. Proposals for photonic integration of microcombs use a comb with an extremely high (~1 THz) repetition rate to achieve the octave-spanning spectrum required for full frequency stabilization [49,50], and a second lower-repetition-rate comb measures the first comb's repetition rate. Generating a breather soliton in the ~1 THz resonator and measuring the frequency of entrained breather oscillations could simplify this system—the locking ratio of $N = 20$ observed with fourth-order dispersion would enable indirect measurement of a 1 THz repetition rate through measurement of entrained oscillations at 50 GHz.

Our investigation of subharmonic entrainment of breather-soliton oscillations to the periodic round-trip-time perturbation in passive, driven, Kerr-nonlinear ring resonators goes beyond what has been investigated experimentally and what can be explored within the LLE model for microcomb dynamics. We expect this proposal of dynamical synchronization across microcomb timescales to open

up a new avenue for research in this field, as to our knowledge effects like this have not yet been investigated. This phenomenon and others like it could prove useful in tailoring microcombs for applications. While it is not yet clear how to realize entrainment of breather oscillations in high-finesse microresonators, this idea could be immediately investigated experimentally using passive fiber-loop "macroring" resonators. These resonators exhibit dynamics that are formally equivalent to those of a microcomb, but have much lower finesse. Many facets of Kerr-nonlinear dynamics have been investigated in fiber loops (e.g. [12,16,51,52]), and they could be a useful test-bed for the theory that we have proposed. We present our results with the hope that they will excite interest in this fundamentally new type of behavior, spur a new course of microcomb research, and prove useful in developing this technology towards maturity.

This work was funded by the DARPA DRINQS program and NIST. We thank Abijith Kowligy and Liron Stern for comments on the manuscript.

*Corresponding author.
daniel.cole@nist.gov

[1] T. J. Kippenberg, A. L. Gaeta, M. Lipson, and M. L. Gorodetsky, Science **361**, eaan8083 (2018).
[2] A. Pasquazi, M. Peccianti, L. Razzari, D. J. Moss, S. Coen, M. Erkintalo, Y. K. Chembo, T. Hansson, S. Wabnitz, P. Del'Haye, X. Xue, A. Weiner, and R. Morandotti, Phys. Rep. **729**, 1 (2018).
[3] K. Y. Yang, K. Beha, D. C. Cole, X. Yi, P. Del'Haye, H. Lee, J. Li, D. Y. Oh, S. A. Diddams, S. B. Papp, and K. J. Vahala, Nat. Photonics **10**, 316 (2016).
[4] V. Brasch, T. Herr, M. Geiselmann, G. Lihachev, M. H. P. Pfeiffer, M. L. Gorodetsky, and T. J. Kippenberg, Science **351**, 357 (2016).
[5] A. A. Savchenkov, A. B. Matsko, W. Liang, V. S. Ilchenko, D. Seidel, and L. Maleki, Opt. Express **20**, 27290 (2012).
[6] T. Herr, V. Brasch, J. D. Jost, I. Mirgorodskiy, G. Lihachev, M. L. Gorodetsky, and T. J. Kippenberg, Phys. Rev. Lett. **113**, 123901 (2014).
[7] X. Yi, Q.-F. Yang, K. Y. Yang, M.-G. Suh, and K. Vahala, Optica **2**, 1078 (2015).
[8] X. Xue, Y. Xuan, Y. Liu, P.-H. Wang, S. Chen, J. Wang, D. E. Leaird, M. Qi, and A. M. Weiner, Nat. Photonics **9**, 594 (2015).
[9] M. Karpov, H. Guo, A. Kordts, V. Brasch, M. H. P. Pfeiffer, M. Zervas, M. Geiselmann, and T. J. Kippenberg, Phys. Rev. Lett. **116**, 103902 (2016).
[10] Y. Okawachi, M. Yu, V. Venkataraman, P. M. Latawiec, A. G. Griffith, M. Lipson, M. Loncar, and A. L. Gaeta, Opt. Lett. **42**, 2786 (2017).
[11] Q. F. Yang, X. Yi, K. Y. Yang, and K. Vahala, Nat. Phys. **13**, 53 (2017).
[12] Y. Wang, M. Anderson, S. Coen, S. G. Murdoch, and M. Erkintalo, Phys. Rev. Lett. **120**, 053902 (2018).
[13] T. Carmon, L. Yang, and K. J. Vahala, Opt. Express **12**, 4742 (2004).
[14] C. Joshi, J. K. Jang, K. Luke, X. Ji, S. A. Miller, A. Klenner, Y. Okawachi, M. Lipson, and A. L. Gaeta, Opt. Lett. **41**, 2565 (2016).
[15] J. R. Stone, T. C. Briles, T. E. Drake, D. T. Spencer, D. R. Carlson, S. A. Diddams, and S. B. Papp, Phys. Rev. Lett. **121**, 063902 (2018).
[16] Y. Wang, F. Leo, J. Fatome, M. Erkintalo, S. G. Murdoch, and S. Coen, Optica **4**, 855 (2017).
[17] D. C. Cole, E. S. Lamb, P. Del'Haye, S. A. Diddams, and S. B. Papp, Nat. Photonics **11**, 671 (2017).
[18] M. Yu, J. K. Jang, Y. Okawachi, A. G. Griffith, K. Luke, S. A. Miller, X. Ji, M. Lipson, and A. L. Gaeta, Nat. Commun. **8**, 14569 (2017).
[19] H. Guo, E. Lucas, M. H. P. Pfeiffer, M. Karpov, M. Anderson, J. Liu, M. Geiselmann, J. D. Jost, and T. J. Kippenberg, Phys. Rev. X **7**, 041055 (2017).
[20] C. Bao, J. A. Jaramillo-Villegas, Y. Xuan, D. E. Leaird, M. Qi, and A. M. Weiner, Phys. Rev. Lett. **117**, 163901 (2016).
[21] E. Lucas, M. Karpov, H. Guo, M. L. Gorodetsky, and T. J. Kippenberg, Nat. Commun. **8**, 736 (2017).
[22] J. M. Dudley, G. Genty, F. Dias, B. Kibler, and N. Akhmediev, Opt. Express **17**, 21497 (2009).
[23] B. Kibler, J. Fatome, C. Finot, G. Millot, F. Dias, G. Genty, N. Akhmediev, and J. M. Dudley, Nat. Phys. **6**, 790 (2010).
[24] B. Van Der Pol and J. Van Der Mark, Nature (London) **120**, 363 (1927).
[25] D. Storti and R. H. Rand, Int. J. Nonlinear Mech. **23**, 231 (1988).
[26] U. Parlitz, L. Junge, and L. Kocarev, Phys. Rev. Lett. **79**, 3158 (1997).
[27] P. M. Varangis, A. Gavrielides, T. Erneux, V. Kovanis, and L. F. Lester, Phys. Rev. Lett. **78**, 2353 (1997).
[28] S. Coen, M. Haelterman, P. Emplit, L. Delage, L. M. Simohamed, and F. Reynaud, J. Opt. Soc. Am. B **15**, 2283 (1998).
[29] J. M. Soto-Crespo, M. Grapinet, P. Grelu, and N. Akhmediev, Phys. Rev. E **70**, 066612 (2004).
[30] N. Y. Yao, A. C. Potter, I.-D. Potirniche, and A. Vishwanath, Phys. Rev. Lett. **118**, 030401 (2017).
[31] S. Choi, J. Choi, R. Landig, G. Kucsko, H. Zhou, J. Isoya, F. Jelezko, S. Onoda, H. Sumiya, V. Khemani, C. von Keyserlingk, N. Y. Yao, E. Demler, and M. D. Lukin, Nature (London) **543**, 221 (2017).
[32] J. Zhang, P. W. Hess, A. Kyprianidis, P. Becker, A. Lee, J. Smith, G. Pagano, I. D. Potirniche, A. C. Potter, A. Vishwanath, N. Y. Yao, and C. Monroe, Nature (London) **543**, 217 (2017).
[33] T. Herr, V. Brasch, J. D. Jost, C. Y. Wang, N. M. Kondratiev, M. L. Gorodetsky, and T. J. Kippenberg, Nat. Photonics **8**, 145 (2014).
[34] L. A. Lugiato and R. Lefever, Phys. Rev. Lett. **58**, 2209 (1987).
[35] A. B. Matsko, A. Savchenkov, W. Liang, V. S. Ilchenko, D. Seidel, and L. Maleki, Opt. Lett. **36**, 2845 (2011).
[36] S. Coen, H. G. Randle, T. Sylvestre, and M. Erkintalo, Opt. Lett. **38**, 37 (2013).
[37] Y. K. Chembo and C. R. Menyuk, Phys. Rev. A **87**, 053852 (2013).

[38] C. Godey, I. V. Balakireva, A. Coillet, and Y. K. Chembo, Phys. Rev. A **89**, 063814 (2014).
[39] See Supplemental Material at http://link.aps.org/supplemental/10.1103/PhysRevLett.123.173904 for normalization of the LLE and Ikeda map, a description of the numerical simulations (which includes Ref. [40]), and a full discussion of the case $\eta = 0.95$.
[40] J. Hult, J. Lightwave Technol. **25**, 3770 (2007).
[41] K. Ikeda, Opt. Commun. **30**, 257 (1979).
[42] M. Haelterman, S. Trillo, and S. Wabnitz, Opt. Commun. **91**, 401 (1992).
[43] A. S. Rogov and E. E. Narimanov, Opt. Lett. **39**, 4305 (2014).
[44] D. C. Cole, Ph.D. thesis, University of Colorado Boulder, 2018, https://scholar.colorado.edu/phys_gradetds/236/.
[45] G. P. Agrawal, *Nonlinear Fiber Optics*, 4th ed. (Elsevier, Burlington, MA, 2007).
[46] R. Adler, Proc. IEEE **61**, 1380 (1973).
[47] G. Di Domenico, S. Schilt, and P. Thomann, Appl. Opt. **49**, 4801 (2010).
[48] C. Bao and C. Yang, Phys. Rev. A **92**, 023802 (2015).
[49] D. T. Spencer *et al.*, Nature (London) **557**, 81 (2018).
[50] T. C. Briles, J. R. Stone, T. E. Drake, D. T. Spencer, C. Fredrick, Q. Li, D. Westly, B. R. Ilic, K. Srinivasan, S. A. Diddams, and S. B. Papp, Opt. Lett. **43**, 2933 (2018).
[51] F. Leo, S. Coen, P. Kockaert, S.-P. Gorza, P. Emplit, and M. Haelterman, Nat. Photonics **4**, 471 (2010).
[52] J. K. Jang, M. Erkintalo, S. G. Murdoch, and S. Coen, Opt. Lett. **40**, 4755 (2015).